

LETTER TO THE EDITOR

The effects of star formation on the low-metallicity ISM: NGC 4214 mapped with *Herschel*^{*}/PACS spectroscopy

D. Cormier¹, S. C. Madden¹, S. Hony¹, A. Contursi², A. Poglitsch², F. Galliano¹, E. Sturm², V. Doublier², H. Feuchtgruber², M. Galametz¹, N. Geis², J. de Jong², K. Okumura¹, P. Panuzzo¹, and M. Sauvage¹

¹ Laboratoire AIM, CEA/DSM - CNRS - Université Paris Diderot, Irfu/Service d'Astrophysique, CEA Saclay, 91191 Gif-sur-Yvette, France
e-mail: diane.cormier@cea.fr

² Max-Planck-Institut fuer extraterrestrische Physik, Postfach 1312, 85741 Garching, Germany

Received 31 March 2010 / Accepted 29 April 2010

ABSTRACT

We present *Herschel*/PACS spectroscopic maps of the dwarf galaxy NGC 4214 observed in 6 far infrared fine-structure lines: [C II] 158 μm , [O III] 88 μm , [O I] 63 μm , [O I] 146 μm , [N II] 122 μm , and [N II] 205 μm . The maps are sampled to the full telescope spatial resolution and reveal unprecedented detail on ~ 150 pc size scales. We detect [C II] emission over the whole mapped area, [O III] being the most luminous FIR line. The ratio of [O III]/[C II] peaks at about 2 toward the sites of massive star formation, higher than ratios seen in dusty starburst galaxies. The [C II]/CO ratios are 20 000 to 70 000 toward the 2 massive clusters, which are at least an order of magnitude larger than spiral or dusty starbursts, and cannot be reconciled with single-slab PDR models. Toward the 2 massive star-forming regions, we find that $L_{[\text{C II}]}$ is 0.5 to 0.8% of the L_{TIR} . All of the lines together contribute up to 2% of L_{TIR} . These extreme findings are a consequence of the lower metallicity and young, massive-star formation commonly found in dwarf galaxies. These conditions promote large-scale photodissociation into the molecular reservoir, which is evident in the FIR line ratios. This illustrates the necessity to move to multiphase models applicable to star-forming clusters or galaxies as a whole.

Key words. galaxies: ISM – galaxies: individual: NGC 4214 – ISM: line and bands – photon-dominated region (PDR) – galaxies: dwarf

1. Introduction

As building blocks of larger galaxies, dwarf galaxies in the early universe presumably played an important role in the evolution of galaxies we see today. Understanding how stars form and evolve under low metallicity conditions and the process of subsequent enrichment of the interstellar medium (ISM) will help us constrain possible scenarios of galaxy formation and evolution. The Local Group dwarf galaxies provide laboratories to study in detail the effects of the lower metal abundance on the process of star formation and the feedback on the ISM.

To examine the interplay between massive star formation and low metallicity ISM, we have mapped the far infrared (FIR) fine structure lines in the Local Group Magellanic-type irregular galaxy, NGC 4214, as part of the *Herschel* key proposal, SHINING (P.I. E. Sturm). NGC 4214 harbors 2 main star-forming complexes containing hundreds of O stars as well as a super star cluster (SSC). Our aim here is to characterise the physical conditions and the structure of the different phases of the ISM in NGC 4214. The proximity of NGC 4214 (2.9 Mpc, [Maíz-Apellániz et al. 2002](#)) and its low-metallicity ($\log(\text{O}/\text{H}) + 12 = 8.2$, [Kobulnicky & Skillman 1996](#)) make it a choice target. The PACS spectrometer onboard the *Herschel* Space Observatory allows us to zoom into the low-metallicity

photodissociation regions (PDRs) and their surroundings, tracing physical properties from 125 to 165 pc size scales.

The tools for this study are the FIR fine-structure lines arising from some of the most abundant species C, O, and N, which provide the most important cooling channels in the neutral and diffuse ionized ISM of galaxies. These lines trace H II regions and PDRs, which are neutral atomic and molecular regions where penetrating FUV photons ($6 \text{ eV} < h\nu < 13.6 \text{ eV}$) dominate the energy balance and the chemical composition of the gas. Most of the ISM in galaxies is contained in PDRs. The FIR lines in combination with PDR models ([Tielens & Hollenbach 1985](#); [Wolfire et al. 1990](#); [Ferland et al. 1998](#); [Kaufman et al. 1999](#); [Abel et al. 2005](#); [Röllig et al. 2006](#)) can unveil the structure of these regions, which depends on both the strength of the FUV radiation field density (G_0) illuminating the cloud and the hydrogen density (n_{H}).

2. Observations and data reduction

We mapped the 6 FIR fine-structure lines, [C II] 158, [O III] 88, [O I] 63, [O I] 146, [N II] 122, and [N II] 205 μm , using the PACS spectrometer ([Poglitsch et al. 2010](#)) on *Herschel* ([Pilbratt et al. 2010](#)). The PACS array consists of 5×5 spatial pixels of $9.4''$ size offering a total field-of-view of $47''$ on the sky. Each spatial pixel covers 16 spectral elements with a spectral resolution ranging from 100 to 300 km s^{-1} . The lines are not spectrally resolved for NGC 4214. The 6 lines were observed in raster mapping mode over a total of 15h during the science demonstration phase. The [O III] 88 μm and [O I] 63 μm (“blue”) were mapped

* *Herschel* is an ESA space observatory with science instruments provided by European-led Principal Investigator consortia and with important participation from NASA.

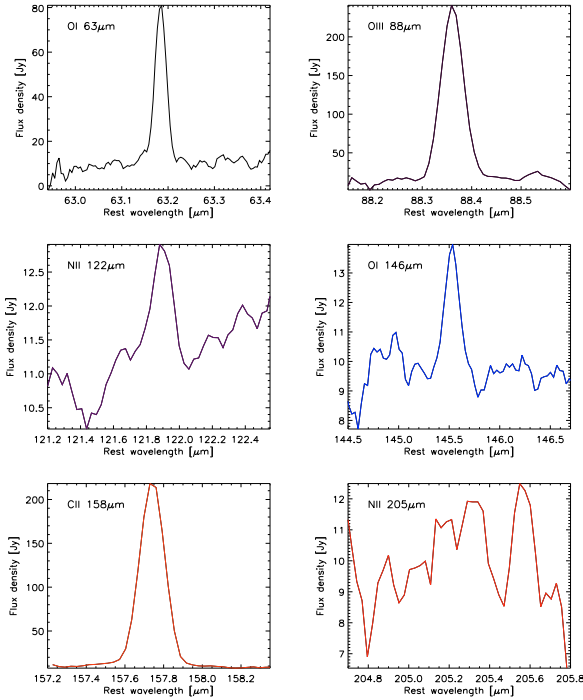


Fig. 1. Individual PACS spectral lines added up over the central raster. The lines are not spectrally resolved.

with 5×5 rasters and the other lines (“red”) with 3×3 rasters, all centered on 12h15m39.08s,+36d19m35.9s (J2000). Each raster pointing is separated by approximately half of the array ($22''$, $24''$) in the “red” range and approximately one third of the array ($14.5''$, $16''$) in the “blue” range, giving homogeneous coverage of the galaxy and a total field of view of $1.6' \times 1.6'$. We selected the chop-nod mode with a chop throw of $6'$ off the source.

The data were reduced with the PACS spectrometer pipeline of the *Herschel* interactive processing environment (HIPE) v3.0.455. We show the 6 individual lines in Fig. 1. We fitted a spline plus Gaussian to the line and baseline and measured the 1σ noise of the residual. In this way, we estimate the overall noise in the maps to be 0.17, 0.42, 0.27, 0.07, 0.06, and 0.30 Jy/pix for the [C II] 158 μ m, [O III] 88 μ m, [O I] 63 μ m, [O I] 146 μ m, [N II] 122 μ m, and [N II] 205 μ m lines, respectively. We applied a flat field correction and divided by calibration correction factors of 1.1 (“red”) and 1.3 (“blue”) to obtain the final reduced maps.

The rasters are combined by a drizzle scheme to produce final maps with $4''$ grid pixel size for the [O III] and [O I] 63 μ m lines, and $6''$ for the other lines. To compare the lines and create ratio maps, we scaled all maps down to the coarser resolution of $6''$. We analyze separately the whole map as well as three specific regions corresponding to NGC 4214-I (center), NGC 4214-II (southeast), and NGC 4214-III (northwest). These are represented by the red circles in Fig. 2a. Regions I and II are centered on the [C II] peaks, with radii encompassing most of the emission (at the level of $\sim 50\%$ of the peak), while region III was chosen by taking into account the peak of the CO emission as well as the brightest counterpart of the [C II] emission ($S/N \geq 15$), which is truncated by the map edge.

3. Results

The *Herschel*/PACS maps clearly resolve the two star-forming regions NGC 4214-I and NGC 4214-II, where most of the emission originates. The [N II] 122 μ m emission is rather faint and the

Table 1. FIR line ratios.

NGC 4214	total	I	II	III
RA [J2000]	12 15 39.1	12 15 39.1	12 15 40.5	12 15 36.7
Dec [J2000]	+36 19 35.9	+36 19 35.9	+36 19 05.9	+36 20 01.0
Aperture ($''$)	–	18	12	9
Quantity	Line ratios			
$f_{\text{[OIII]}}/f_{\text{[CII]}}$	0.996 (0.009)	1.40 (0.007)	1.71 (0.014)	0.264 (0.053)
$f_{\text{[OI]146}}/f_{\text{[OI]63}}$	0.058 (0.015)	0.060 (0.011)	0.072 (0.023)	– (0.095)
$f_{\text{[OI]63}}/f_{\text{[CII]}}$	0.445 (0.007)	0.474 (0.004)	0.560 (0.008)	0.438 (0.035)
$f_{\text{[OI]146}}/f_{\text{[CII]}}$	0.026 (0.007)	0.028 (0.005)	0.040 (0.013)	– (0.042)
$L_{\text{TIR}} [10^7 L_{\odot}]$	37.7	8.60	4.52	0.522
$10^{-3} L_{\text{[OI]63}} + L_{\text{[CII]}} / L_{\text{TIR}}$	2.77	8.11	6.50	11.1
$10^{-3} L_{\text{[CII]}} / L_{\text{TIR}}$	5.30	7.93	5.71	7.70
$10^3 L_{\text{[CII]}} / L_{\text{CO}}$	33.8	75.0	22.9	4.73

[N II] 205 μ m is not detected. The most prominent lines are the [C II] 158 μ m, [O III] 88 μ m, [O I] 63 μ m, and, to a lesser extent, the [O I] 146 μ m and [N II] 122 μ m lines. The emission from the [C II] line is the most extended of all of the lines (Fig. 2a) and covers the entire map. The total [C II] luminosity in the PACS map is $2.0 \times 10^6 L_{\odot}$ with about 50% of the emission originating in the two bright star-forming sites and 50% in the surrounding medium. The [C II] 158 μ m line is known to be one of the most important tracers of physical conditions in PDRs because it is so luminous and has a low critical density for collisional excitation.

Comparing the [C II] and [O I] 63 μ m line emission, we find that the latter is a factor of two weaker integrated over the mapped region. These two lines show a very similar distribution (Fig. 2b), both peaking at the 2 star-forming sites and spanning a small range of ratios. These ratios vary by less than a factor of two across the entire map. The [C II] line, in principle, may originate in the PDR and the diffuse media alike. The observed resemblance between the [O I] 63 μ m and [C II] maps (Fig. 2b) suggests that the [C II] is dominated by the PDR component (see also Sect. 3.1).

The [O I] 146 μ m line is fainter than the [O I] 63 μ m line, and is barely detected in the outer regions of the map. Toward the 2 peaks, and in total, the ratios of the two [O I] lines are about 0.06 (Table 1), and do not vary much across the map. These ratios are insensitive to density since their critical densities are not very different. For moderate densities ($n < 10^5 \text{ cm}^{-3}$), this ratio is more indicative of the gas temperature.

The [O III] 88 μ m line is the brightest of all lines observed in NGC 4214 (Fig. 2c). A comparison of the [O III] line map with the *HST* optical images of NGC 4214 (Úbeda et al. 2007), illustrates that it coincides with the star formation sites and exhibits a peak toward the position of the SSC in NGC 4214-I, thus tracing the ionization source. High ratios of [O III] to [C II] observed here (Table 1) are not commonly seen in dusty starbursts or spiral galaxies (Negishi et al. 2001; Malhotra et al. 2001), an example being M82 with a ratio of ~ 0.7 . However, high ratios have been observed in the *ISO* observations of dwarf galaxies and may be explained by hot stars surrounded by optically thick PDRs (Hunter et al. 2001). The [O III] / [C II] ratio map of NGC 4214 (Fig. 2d) exhibits peaks in intensity toward the 2 star-forming sites but drops off rapidly away from the peaks. We note that the peaks of the [O III] / [C II] ratio map appear to be offset from those of the [C II] by $\sim 6''$, which is larger than the expected relative pointing uncertainty (on the order of several arcsecs).

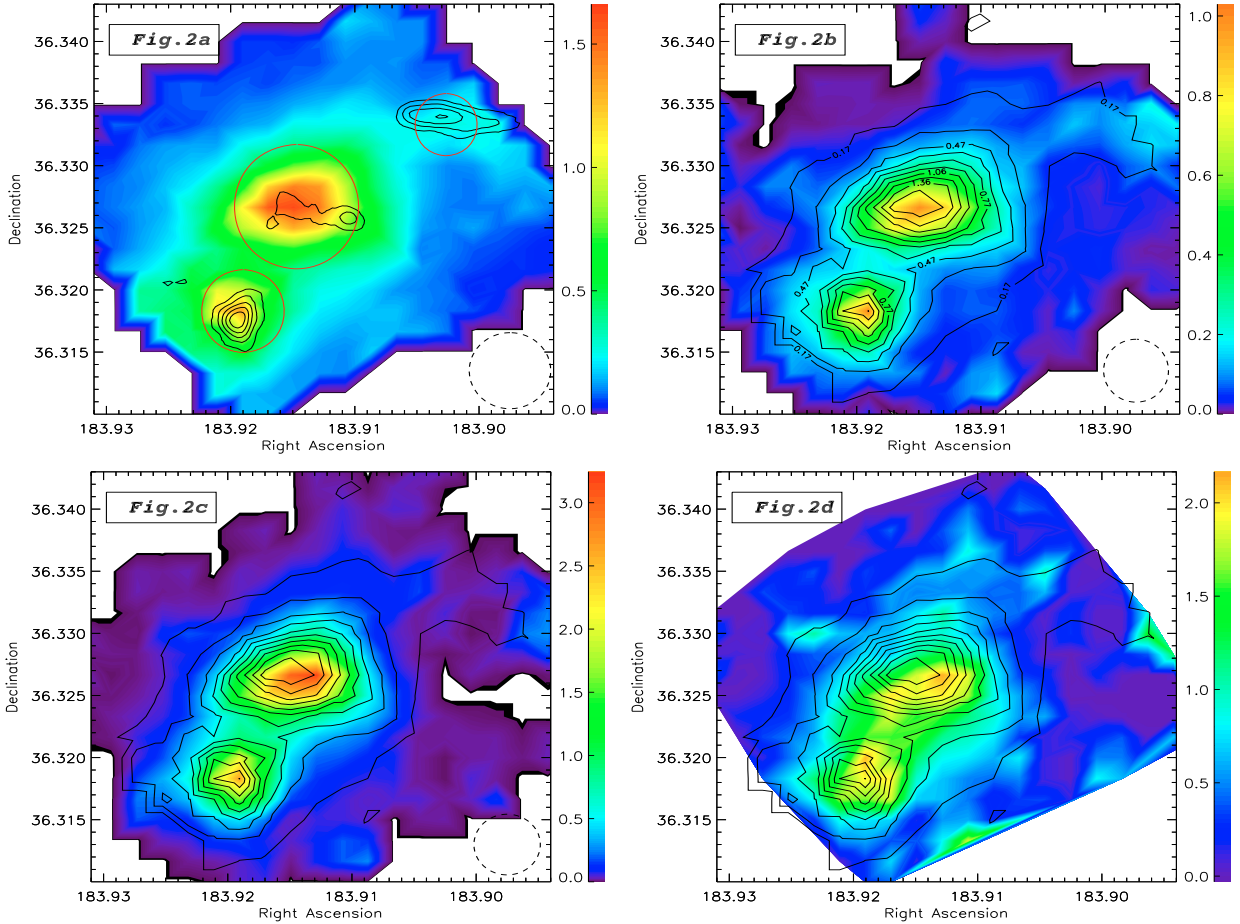


Fig. 2. PACS spectral maps of NGC 4214. **a)** PACS map of the [C II] 158 μm line with CO(1–0) contours (Walter et al. 2001). The total field of view is $1.6' \times 1.6'$ with a grid resolution of $6''$. The red circles show the positions and sizes of the 3 regions we study in more detail: NGC 4214-I (center – $36''$ diameter), NGC 4214-II (southeast – $24''$), and NGC 4214-III (northwest – $18''$). The dotted circle on the lower right corner represents the PACS beam size of $9.4'' \times 9.1''$ at $62 \mu\text{m}$, $9.6'' \times 8.8''$ at $90 \mu\text{m}$, and $11.8'' \times 11.0''$ at $154 \mu\text{m}$. **b)** PACS map of the [O I] 63 μm line with [C II] 158 μm contours. **c)** PACS map of the [O III] 88 μm line with [C II] 158 μm contours. **d)** Ratio map of [O III] 88 μm /[C II] with [C II] contours. Units for the color bars are $10^{-16} \text{ W m}^{-2} \text{ grid pix}^{-1}$. The [C II] contours begin at $0.17 \times 10^{-16} \text{ W m}^{-2}$ (above 15σ) and are linearly spaced up to the peak of $1.66 \times 10^{-16} \text{ W m}^{-2}$.

The shift in the [O III] / [C II] peak, corresponding to a shift of $\sim 80 \text{ pc}$, if real, implies that the ratio peak coincides with the SSC peak, the probable source of the ionization. Since O^{++} has an ionization potential of 35.1 eV, [O III] traces the highly ionized medium around early O stars and is thus more confined than the [C II] emission. This is consistent with the AKARI findings that the [O III] 88 μm line traces excitation sources even more accurately than the radio continuum (Okada et al. 2010).

We show the CO contours from Walter et al. (2001) in Fig. 2a. There is a striking distinction between the three different regions in terms of [C II]/CO (Table 1). NGC 4214-III probably hosts little star formation, which explains its paucity in excited FIR line emission compared to its molecular reservoir. However, even the two main regions of active star formation exhibit very different [C II]/CO ratios. One explanation of these high [C II]/CO ratios is the presence of small clumps of CO embedded in large PDR envelopes. Applying this interpretation to these observations would imply that the star formation in the central region of NGC 4214-I has (already) affected (photodissociated) most of the surrounding molecular reservoir, while many of the molecular clouds in the south eastern region are relatively unscathed. It is interesting to remark that NGC 4214-II has a younger stellar population than NGC 4214-I (Úbeda et al. 2007).

Using *Spitzer* data, we estimate the total infrared luminosity (L_{TIR}) over the area mapped with PACS, following

Dale & Helou (2002) (see Table 1). The [C II] line alone accounts for $\sim 0.5\%$ of the L_{TIR} ¹, which is at the high end of the range of normal galaxies and starburst galaxies (Stacey et al. 1991; Negishi et al. 2001) and more typical of the elevated ratios seen in dwarf galaxies (Madden 2000; Hunter et al. 2001). Toward the two bright star-forming regions, $L_{[\text{CII}]} / L_{\text{TIR}}$ is similar to 30 Dor in the LMC (Poglitsch et al. 1995; Rubin et al. 2009). Likewise, $L_{[\text{OIII}]} / L_{\text{TIR}}$ either toward these 2 prominent star-forming regions or over the entire galaxy is an order of magnitude higher than what Negishi et al. (2001) find for normal and starburst galaxies. The FIR lines of the 2 star-forming regions contribute all together up to about 2% of their TIR flux.

3.1. Origin of the [C II] line

Before we can consider PDR model solutions to the observations, we consider the origin of the C^+ line, which is most often used as a diagnostic of PDR conditions because it is a primary coolant in PDRs. However, since the ionization potential of carbon (11.3 eV) is less than that of hydrogen, C^+ can exist in both the ionized and neutral gas. In galactic nuclei, most of the [C II] emission arises from the PDRs (Stacey et al. 1991;

¹ To compare ratios using L_{FIR} in the literature, for dwarf galaxies (Hunter et al. 2001), L_{TIR} is approximately a factor of 2 greater than L_{FIR} , as defined by IRAS 60 and 100 μm fluxes (Helou et al. 1988).

Negishi et al. 2001). With an ionization potential of 14.53 eV, the N^+ emission originates only from the H II regions. Therefore we use the [N II] line to correct for a possible contribution of the ionized gas to the C^+ line.

The [N II] 205 μm line was not confidently detected and could not be analyzed but the [N II] 122 μm line is detected in the two star-forming regions. We see evidence of [N II] 122 μm emission over the central 3×3 pixels in each region and average them to obtain a higher signal-to-noise ratio and measure the intensity of the line in these two regions. The observed ratios of the [N II] 122 μm /[C II] 158 μm are 0.04 and 0.03 in NGC 4214-I and NGC 4214-II, respectively. Following Malhotra et al. (2001), we estimate a maximum contribution of the ionized medium to the [C II] emission to be a factor of 11 times the flux of the [N II] 122 μm . Therefore, at least 60% of the [C II] emission originates in PDRs. To bound the physical conditions in NGC 4214, we model the PDR (see Sect. 3.2) assuming that all [C II] emission is from PDRs and that only 60% originates in PDRs.

3.2. Results from PDR models

As a first diagnostic of PDR properties, we use the model of Kaufman et al. (1999) by means of the web interface of the PDR Toolbox². This model, which assumes solar metallicity, calculates the intensity of the main PDR lines as a function of the physical conditions, which are the incident radiation field (G_0) and the density (n_H). We can compare our observed line intensities to the model predictions to narrow down the range of the physical conditions.

We use [O I] 63 μm /[C II], [O I] 146 μm /[C II], [O I] 146 μm /[O I] 63 μm , and the $([C II] + [O I] 63 \mu\text{m})/I_{\text{TIR}}$ and [C II]/CO (Table 1). The ratio $([C II] + [O I] 63 \mu\text{m})/I_{\text{TIR}}$ is interesting because it relates the “total” cooling of the gas to the total cooling by the dust, so measures the efficiency of the dust to heat the gas (photoelectric efficiency). The observed [C II]/CO ratio disagrees significantly with those predicted by the best-fit solution for all the other line ratios. This has been noted before for other low metallicity PDRs (see Sect. 3.3) and may be a geometry or low metallicity effect not taken into account in the model. Using all the above line ratios except [C II]/CO, the maximum values found for NGC 4214-I are $G_0^3 \sim 800$ and $n_H \sim 2000$. For NGC 4214-II, we find that $G_0 \sim 1000$ and $n_H \sim 3000$. The solution for the third region NGC 4214-III infers a lower incident radiation field ($G_0 \lesssim 100$). The quoted values above take into account the contribution to the [C II] intensity of the ionized medium between 0 and 40%. In all cases, these PDR parameters are indicative of a relatively moderate gas density and radiation field.

3.3. [C II]-to-CO ratio

We measure [C II]/CO intensity ratios of 70 000 and 20 000 for NGC 4214-I and II, respectively (Table 1). These values are at least an order of magnitude higher than those inferred for spiral or starburst galaxies (Stacey et al. 1991; Negishi et al. 2001) but in closer agreement with those of dwarf galaxies (Poglitsch et al. 1995; Madden et al. 1997; Hunter et al. 2001). NGC 4214-I has a [C II]/CO similar to 30 Dor (Poglitsch et al. 1995; Rubin et al. 2009). This high ratio could be explained by the paucity of dust; less dust shielding allows the photodissociating FUV photons to penetrate deeper into the cloud, reducing the size of

the CO cores while leaving a large [C II]-emitting envelope. This envelope may well contain self-shielded molecular hydrogen. If this were true, the [C II] would be a more accurate tracer of the molecular reservoirs in low metallicity environments than CO.

4. Conclusion

These observations of NGC 4214 with *Herschel*/PACS have enabled us to spatially resolve the FIR fine-structure lines in the low metallicity dwarf galaxy NGC 4214. A very striking result from the mapping is the brightness of the [C II] 158 μm , [O I] 63 μm , and the [O III] 88 μm lines. The [C II] alone corresponds to 0.5% of the total infrared luminosity. The combined luminosity of the FIR lines reaches 2% of the L_{TIR} . The [O III] 88 μm line is more confined to star-forming regions and the [O III]/[C II] reaches almost a factor of 2 close to the SSC in NGC 4214-I.

The [C II]/CO ratios are also exceptionally high (20 000–70 000). These extreme ratios are indicative of an ISM that is strongly affected by photodissociation and reflect the combined effects of low metallicity ISM and intense star formation. It should be borne in mind that, when comparing with models, the models predict line ratios for a single, homogeneous PDR. In reality, we observe a multiphase medium that probably harbors many extremely different PDR conditions. Therefore, this preliminary comparison indicates the need for more complete (complex) models to be able to derive accurate physical quantities.

Acknowledgements. We would like to thank the referee for suggestions that improved this letter. Many thanks to Fabian Walter for sharing his valuable CO data with us, and Leonardo Úbeda for his HST images for us to compare with. We are also extremely grateful for the help of the PACS ICC and *Herschel* Science Centre. PACS has been developed by a consortium of institutes led by MPE (Germany) and including MPE (Austria); KU Leuven, CSL, IMEC (Belgium); CEA, LAM (France); MPIA (Germany); INAF-IFSI/OAA/OAP/OAT, LENS, SISSA (Italy); IAC (Spain). This development has been supported by the funding agencies BMVIT (Austria), ESA-PRODEX (Belgium), CEA/CNES (France), DLR (Germany), ASI/INAF (Italy), and CICYT/MCYT (Spain).

References

- Abel, N. P., Ferland, G. J., Shaw, G., & van Hoof, P. A. M. 2005, *ApJS*, 161, 65
- Dale, D. A., & Helou, G. 2002, *ApJ*, 576, 159
- Ferland, G. J., Korista, K. T., Verner, D. A., et al. 1998, *PASP*, 110, 761
- Helou, G., Khan, I. R., Malek, L., & Boehmer, L. 1988, *ApJS*, 68, 151
- Hunter, D. A., Kaufman, M., Hollenbach, D. J., et al. 2001, *ApJ*, 553, 121
- Kaufman, M. J., Wolfire, M. G., Hollenbach, D. J., & Luhman, M. L. 1999, *ApJ*, 527, 795
- Kobulnicky, H. A., & Skillman, E. D. 1996, *ApJ*, 471, 211
- Madden, S. C. 2000, *New Astron. Rev.*, 44, 249
- Madden, S. C., Poglitsch, A., Geis, N., Stacey, G. J., & Townes, C. H. 1997, *ApJ*, 483, 200
- Maíz-Apellániz, J., Cieza, L., & MacKenty, J. W. 2002, *AJ*, 123, 1307
- Malhotra, S., Kaufman, M. J., Hollenbach, D., et al. 2001, *ApJ*, 561, 766
- Negishi, T., Onaka, T., Chan, K., & Roellig, T. L. 2001, *A&A*, 375, 566
- Okada, Y., Kawada, M., Murakami, N., et al. 2010, *A&A*, 514, A13
- Pilbratt, G. L., et al. 2010, *A&A*, 518, L1
- Poglitsch, A., Krabbe, A., Madden, S. C., et al. 1995, *ApJ*, 454, 293
- Poglitsch, A., et al. 2010, *A&A*, 518, L2
- Röllig, M., Ossenkopf, V., Jeyakumar, S., Stutzki, J., & Sternberg, A. 2006, *A&A*, 451, 917
- Rubin, D., Hony, S., Madden, S. C., et al. 2009, *A&A*, 494, 647
- Stacey, G. J., Geis, N., Genzel, R., et al. 1991, *ApJ*, 373, 423
- Tielens, A. G. G. M., & Hollenbach, D. 1985, *ApJ*, 291, 722
- Úbeda, L., Maíz-Apellániz, J., & MacKenty, J. W. 2007, *AJ*, 133, 917
- Walter, F., Taylor, C. L., Hüttemeister, S., Scoville, N., & McIntyre, V. 2001, *AJ*, 121, 727
- Wolfire, M. G., Tielens, A. G. G. M., & Hollenbach, D. 1990, *ApJ*, 358, 116

² <http://dustem.astro.umd.edu/pdrt/index.html>

³ In units of Habing field: $1.6 \times 10^{-3} \text{ erg cm}^{-2} \text{ s}^{-1}$.